High-Resolution Three-Dimensional Structure of Interleukin 1β in Solution by Three- and Four-Dimensional Nuclear Magnetic Resonance Spectroscopy†,‡

G. Marius Clore,*,§ Paul T. Wingfield,‖ and Angela M. Gronenborn*,§

Laboratory of Chemical Physics, Building 2, National Institute of Diabetes and Digestive and Kidney Diseases, and Protein Expression Laboratory, Building 6B, National Institutes of Health, Bethesda, Maryland 20892

Received November 30, 1990; Revised Manuscript Received January 8, 1991

ABSTRACT: The determination of the high-resolution three-dimensional solution structure of interleukin 1β (IL-1β), a protein of 153 residues and 17.4 kDa, which plays a central role in the immune and inflammatory responses, has been determined by heteronuclear (^{13}C and ^{15}N) three- and four-dimensional NMR spectroscopy. The structure is based on 3146 experimental restraints comprising 2780 distance and 366 torsion angle (ϕ, ψ, and χ_1) restraints. A total of 32 simulated annealing structures are calculated, and the atomic RMS distribution about the mean coordinate positions is 0.41 ± 0.04 Å for the backbone atoms and 0.82 ± 0.04 Å for all atoms (excluding residue 1 at the N-terminus and residues 152 and 153 at the C-terminus, which are partially disordered). In the case of internal side chains with a surface accessibility of ≤40%, the atomic RMS distribution about the mean coordinate positions for all atoms is 0.49 ± 0.03 Å. IL-1β resembles a tetrahedron and is composed of 12 β-strands arranged in three pseudosymmetric topological units, each of which comprises 5 strands. Analysis of the mutational data on IL-1β in the light of the three-dimensional structure suggests the presence of three distinct binding sites for the IL-1 receptor on the surface of the protein. It is suggested that each of the three immunoglobulin domains which comprise the extracellular portion of the IL-1 receptor recognizes one of these sites.

Interleukin 1β (IL-1β)[1] is a protein of 153 residues and 17.4 kDa that plays a central role in the immune and inflammatory responses [see Dinarello (1989) for a review]. Its wide-ranging biological activities include the stimulation of B-lymphocyte proliferation, thymocyte proliferation via the induction of interleukin 2 release, prostaglandin and collagenase release, and stimulation of interleukin 2 and c-jun transcription. As part of a research effort designed to elucidate structure–function relationships in IL-1β, we have been engaged over the past five years in a long-term NMR study with the eventual aim of determining its solution structure at high resolution.

In terms of the number of residues, IL-1β is about 1.5 times larger than the largest protein structures determined to date by NMR, namely, those of *Escherichia coli* (Dyson et al., 1990) and human (Forman-Kay et al., 1991) thioredoxin (108 and 105 residues, respectively). Because of its large size, a solution structure determination of IL-1β by NMR presents a formidable problem. Indeed, conventional 2D NMR methods could not be applied successfully to IL-1β owing to extensive spectral overlap, as well as problems associated with increased line widths commonly found for proteins in the 15–20 kDa range. In a series of recent papers, we therefore developed and exploited a range of 3D heteronuclear double- and triple-resonance NMR experiments to obtain complete ^1H, ^{15}N, and ^{13}C resonance assignments for both the backbone (Driscoll et al., 1990a) and side chains (Clore et al., 1990a), to delineate elements of regular secondary structure (Driscoll et al., 1990b), to identify and localize bound water molecules (Clore et al., 1990b), and to analyze the backbone dynamics (Clore et al., 1990c). In addition, we were able to determine a low-resolution 3D structure on the basis of a small number of NOEs (446) involving solely backbone protons derived principally from a 3D ^{15}N-edited NOESY spectrum (Clore et al., 1990d). However, even with 3D ^{15}N- and ^{13}C-edited NOESY spectra in hand, we were unable to unambiguously assign a large enough number of NOEs to permit the determination of a high-resolution structure of the quality now attainable for small proteins (Kraulis et al., 1989; Qian et al., 1989; Clore et al., 1990e). To resolve this impasse, we resorted to increasing the dimensionality of the spectra still further and recently demonstrated the feasibility of both 4D $^{15}N/^{13}C$- and $^{13}C/^{13}C$-edited NOESY spectroscopy to virtually completely remove ambiguities in the assignment of NOEs (Kay et al., 1990; Clore et al., 1991a). The present paper represents the culmination of these efforts and describes the determination of a high-resolution structure of IL-1β in solution based on heteronuclear 3D and 4D NMR spectroscopy.

Experimental Procedures

Uniformly (>95%) ^{15}N- and/or ^{13}C-labeled protein was prepared and purified as described previously (Gronenborn et al., 1986; Clore et al., 1990a). All samples for NMR contained 1.7 mM protein in either 90 mM phosphate buffer, pH 5.4, or 150 mM sodium acetate-d_3 buffer, pH 5.4, dissolved in either 90% H_2O/10% D_2O or 99.996% D_2O. All spectra were recorded on a Bruker AM600 spectrometer at 36 °C, and examples of the quality of the spectra are found in previous publications (Driscoll et al., 1990a,b; Clore et al., 1990a,b, 1991a,b; Kay et al., 1990). NOEs were assigned from 3D and 4D heteronuclear edited NOESY spectra recorded with mixing times ranging from 80 to 110 ms [i.e., 3D ^1H–^{15}N NOESY-HMQC (Marion et al., 1989a,b; Zuiderweg & Fesik, 1989), ^1H–^{13}C NOESY-HMQC (Ikura et al., 1990; Zuiderweg et al., 1990), 4D $^{15}N/^{13}C$-edited NOESY (Kay et al., 1990), and

† This work was supported by the AIDS-Directed Anti-Viral Program of the Office of the Director of the National Institutes of Health.

‡ The coordinates of the 32 simulated annealing structures and of the restrained minimized mean structure (SA)r, together with the experimental restraints, have been deposited in the Brookhaven Protein Data Bank (PDB code numbers 7I1B, 6I1B, and R6I1BNMR, respectively).

§ Laboratory of Chemical Physics.

‖ Protein Expression Laboratory.

[1] Abbreviations: IL-1β, interleukin 1β; NOE, nuclear Overhauser effect; NOESY, nuclear Overhauser enhancement spectroscopy; HOHAHA, homonuclear Hartmann–Hahn spectroscopy; HMQC, heteronuclear multiple-quantum coherence; 2D, two dimensional; 3D, three dimensional; 4D, four dimensional.

4D $^{13}C/^{13}C$-edited NOESY (Clore et al., 1991a)]. In the case of intraresidue NOEs, we made use of 3D $^{1}H-^{15}N$ ROESY-HMQC (Clore et al., 1990b) and 3D $^{1}H-^{13}C$ ROESY-HMQC (Clore et al., 1991b) spectra recorded with mixing times of 33 and 22 ms, respectively, as well as some short mixing time (30–50 ms) $^{1}H-^{15}N$ and $^{1}H-^{13}C$ NOESY-HMQC spectra. $^{3}J_{HN\alpha}$ coupling constants were obtained from an HMQC-J spectrum (Kay & Bax, 1990), as reported previously (Driscoll et al., 1990b). $^{3}J_{\alpha\beta}$ coupling constants were either obtained from a 2D $^{1}H-^{1}H$ PE-COSY (Mueller, 1987) spectrum in those cases where the $C^{\alpha}H-C^{\beta}H$ cross peaks were sufficiently well resolved to measure the passive couplings from the reduced multiplets or ascertained in a semiquantitative manner (Clore et al., 1991b) from the relative intensities of the $NH-C^{\beta}H$ cross peaks in a 3D $^{1}H-^{15}N$ HOHAHA-HMQC spectrum recorded with a 30.7-ms DIPSI-2 (Shaka et al., 1988) mixing sequence. The semiquantitative analysis was sufficient to assess whether the $^{3}J_{\alpha\beta}$ coupling was <4 Hz, >10 Hz, or between 6 and 8 Hz, the latter being indicative of conformational averaging (Clore et al., 1991b).

The NOEs were classified into strong, medium, and weak corresponding to interproton distance restraints of 1.8–2.7, 1.8–3.3 (1.8–3.5 Å for NOEs involving NH protons), and 1.8–5.0 Å, respectively (Clore et al., 1986). Upper distance limits for distances involving methyl protons and nonstereospecifically assigned methylene protons were corrected appropriately for center averaging (Wüthrich et al., 1983), and an additional 0.5 Å was added to the upper distance limits for NOEs involving methyl protons (Clore et al., 1987). Stereospecific assignments and ϕ, ψ, and χ_1 torsion angle restraints were derived on the basis of sequential and intraresidue NOEs and the $^{3}J_{HN\alpha}$ and $^{3}J_{\alpha\beta}$ coupling constants by using the conformational grid search program STEREOSEARCH (Nilges et al., 1990). The minimum ranges employed for ϕ, ψ, and χ_1 torsion angle restraints were ±30°, ±50°, and ±20°, respectively (Kraulis et al., 1989).

The structures were calculated by using the hybrid distance geometry–dynamical simulated annealing method of Nilges et al. (1988) with a few minor modifications (Clore et al., 1990d,e). This makes use of the program DISGEO (Havel, 1986) to calculate an initial set of substructures comprising about a third of the atoms by projection from *n*-dimensional distance space into Cartesian coordinate space, followed by simulated annealing including all atoms with the program XPLOR (Brünger, 1988). As in previous NMR structure determinations from this laboratory (Kraulis et al., 1989; Clore et al., 1990e; Forman-Kay et al., 1991), an iterative procedure was employed. At the end of this process, all slowly exchanging NH protons could be accounted for by specific hydrogen bonds, and stereospecific assignments were obtained for 81 of the 121 residues with β-methylene protons, for all α-methylene protons of Gly, for the methyl groups of 10 of the 11 Val residues, and for the methyl groups of 12 of the 13 Leu residues. It should also be noted that, in the case of the majority of residues for which stereospecific assignments of β-methylene protons could not be obtained, the $^{3}J_{\alpha\beta}$ couplings were in the 6–8-Hz range and the STEREOSEARCH (Nilges et al., 1990) program was unable to find any χ_1 torsion angles compatible with the NMR data. Both these observations are indicative of multiple side-chain conformations, and not surprisingly, these residues were found to be located on the surface of the protein. At the very final stage of the refinement process, 7 of the 11 bound water molecules that had been identified previously by 3D ^{15}N-edited ROESY spectroscopy (Clore et al., 1990b) were added (see Results and Discussion).

The final structures were computed on the basis of 3146 experimental restraints. These comprised a total of 2630 interproton distance restraints, 114 distance restraints for 57 hydrogen bonds, 36 distance restraints relating to hydrogen bonds involving the 7 bound water molecules, and 366 torsion angle restraints (involving 152 ϕ, 115 ψ, and 99 χ_1 torsion angles). Of the 57 hydrogen bonds, 55 involved backbone NH···CO hydrogen bonds in β-sheets and β-turns. The remaining two involved side-chain to backbone NH hydrogen bonds in a turn between the carboxylate group of Asp-12 and the NH protons of Gln-14 and Lys-16.

Results and Discussion

The Converged Structures. A total of 32 final simulated annealing structures were obtained. The structural statistics are given in Table I, and superpositions of the backbone atoms are shown in Figure 1. With the exception of residue 1 at the N-terminus and residues 152 and 153 at the C-terminus, which are partially disordered, the structure is exceptionally well defined with a backbone atomic RMS distribution of the individual structures about the mean coordinate positions of 0.41 ± 0.04 Å (cf. Figure 2A). In addition, the average angular RMS difference for the ϕ and ψ torsion angles is 9.1 ± 7.3°, and all the backbone torsion angles lie within the allowed regions of the Ramachandran plot (Figure 2B). In this regard it should be noted that, in addition to some Gly residues, a number of Asp and Asn residues have positive ϕ angles, and all of these residues are located in turns. The largest backbone deviations occur in the loop regions (cf. Figures 1 and 2A) and are associated with hinge motions involving one or two residues rather than an increase in local disorder. For example, the increase in the atomic RMS distribution for residues 31–36 (Figure 2A) is due to an increase in the angular RMS difference for the ψ angle of residues 30 and 36 and the ϕ angle of residue 31. Similarly, in the case of residues 48–55, much of the increase in atomic RMS distribution can be attributed to the increase in the angular RMS difference for ψ of residue 51 and ϕ of residue 52. The internal side chains are also very well defined, and the atomic RMS distribution about the mean coordinate positions is 0.49 ± 0.03 Å for all atoms of residues exhibiting ≤40% surface accessibility. Not surprisingly, surface side chains, and in particular residues with longer side chains such as Lys and Arg, tend to be partially disordered, especially beyond the C^{γ} position.

Description of the Structure. The overall structure resembles a tetrahedron and displays internal 3-fold pseudosymmetry. There are 12 β-strands arranged in an exclusively antiparallel β-structure (Table II). Six strands (strands I, IV, V, VIII, IX, and XII) form a β-barrel, which is closed off at the back of the molecule by the other six strands. All the strands are regular with the exception of strand IV, which has a β-bulge from residues 46 to 49. Each repeating topological unit comprises five strands arranged in an antiparallel manner with respect to each other, and best fit superpositions of the backbone atoms of the three topological units together with the interface between them are shown in Figure 3. The backbone hydrogen bonding is essentially identical with that previously described on the basis of a qualitative interpretation of the NOE data (Driscoll et al., 1990b).

Three pairs of strands are connected by classical four-residue β-turns: namely, strands I and II by a type I turn (residues 12–15) and strands VI and VII and strands VIII and IX by type I′ turns (residues 74–77 and 106–109, respectively). Another five pairs of strands are joined by irregular turns and/or short loops of five to six residues. These comprise the connections between strands II and III (residues 21–25), IV and V (residues 51–55), V and VI (residues 62–67), X and XI (residues 125–130), and XI and XII (residues 136–141). In each of these cases, at least one peptide segment of the same

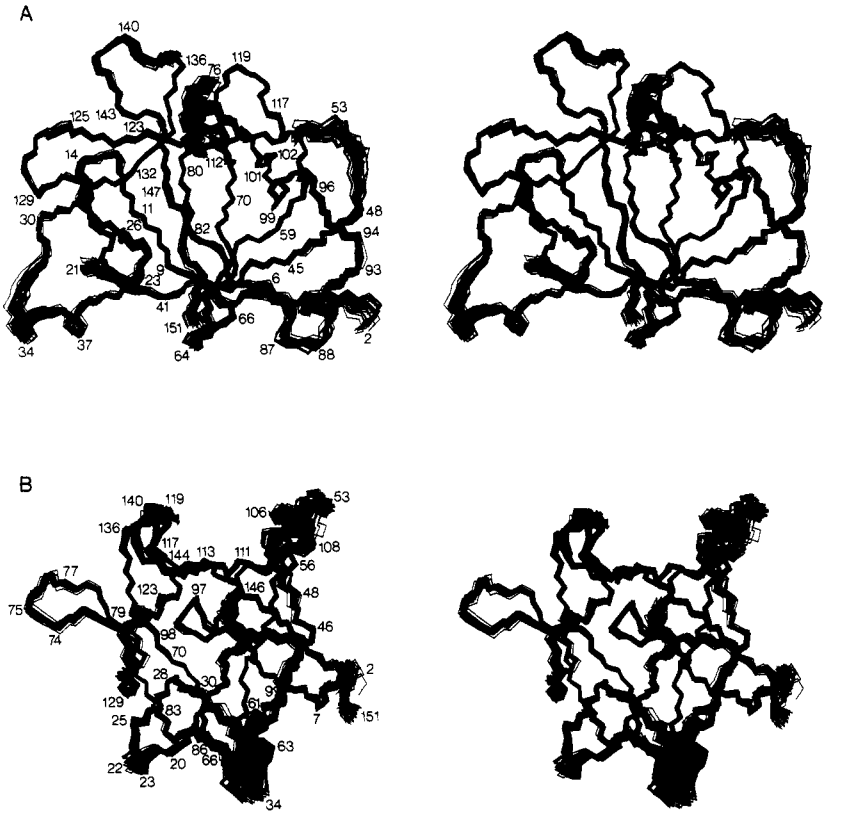

FIGURE 1: Two stereoviews showing best fit superpositions of the backbone (N, C^{α}, C) atoms of the 32 SA structures.

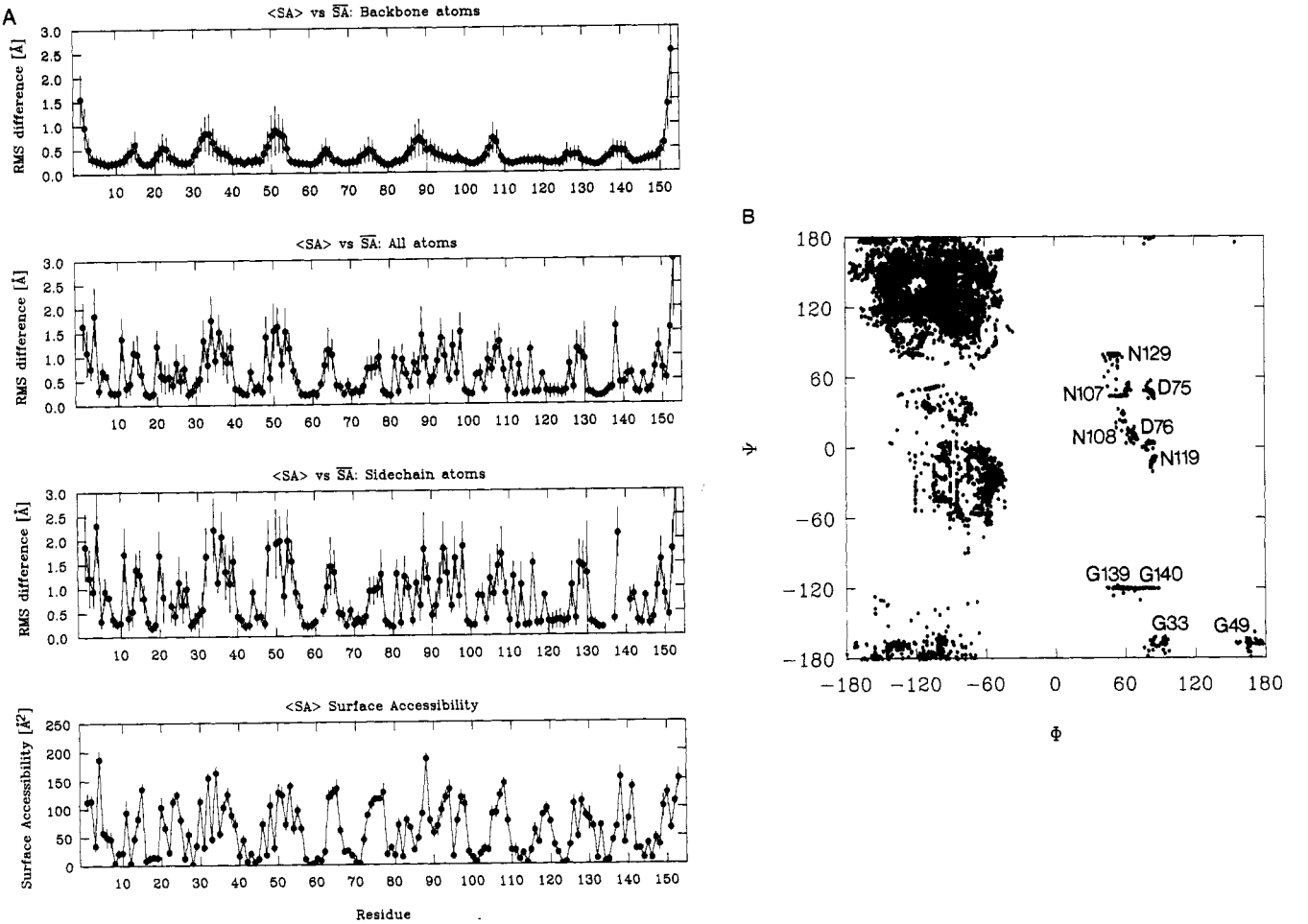

FIGURE 2: (A) Atomic RMS distribution of the 32 individual SA structures about the mean structure $\overline{SA}$, together with the variation in surface accessibility, as a function of residue number. The filled-in circles represent the average values at each residue and the bars the standard deviations in these values. (B) Ramachandran ϕ, ψ plot for the 32 SA structures.

Table I: Structural Statistics and Atomic RMS Differences[a]

structural statistics	⟨SA⟩	(SA)r
RMS deviations from exptl distance restraints (Å)[b]		
all (2780)	0.026 ± 0.0007	0.027
interproton distances		
interresidue sequential ($\|i-j\|=1$) (592)	0.027 ± 0.002	0.031
interresidue short range ($1<\|i-j\|\leq 5$) (265)	0.024 ± 0.003	0.025
interresidue long range ($\|i-j\|>5$) (848)	0.023 ± 0.002	0.024
intraresidue (925)	0.028 ± 0.002	0.027
H-bonds (114)[c]	0.026 ± 0.003	0.027
bound water (36)[c]	0.004 ± 0.007	0.000
RMS deviations from exptl dihedral restraints (deg) (366)[b]	0.190 ± 0.024	0.199
F_{NOE} (kcal·mol^{-1})[d]	56 ± 3	59
F_{tor} (kcal·mol^{-1})[d]	0.89 ± 0.23	0.95
F_{repel} (kcal·mol^{-1})[d]	38 ± 2	57
E_{L-J} (kcal·mol^{-1})[e]	−570 ± 11	−561
deviations from idealized covalent geometry		
bonds (Å) (2474)	0.005 ± 0	0.005
angles (deg) (4469)	1.868 ± 0.002	2.109
impropers (deg) (929)	0.523 ± 0.006	0.556

	residues 2–151		internal residues (≤40% surface accessible)[f]	
atomic RMS differences	backbone atoms	all atoms	backbone atoms	all atoms
⟨SA⟩ vs $\overline{SA}$	0.41 ± 0.04	0.82 ± 0.04	0.28 ± 0.03	0.49 ± 0.03
(SA)r vs $\overline{SA}$	0.13	0.39	0.09	0.25
⟨SA⟩ vs (SA)r	0.43 ± 0.04	0.90 ± 0.04	0.29 ± 0.03	0.55 ± 0.04

[a] The notation of the structures is as follows: ⟨SA⟩ are the final 32 simulated annealing structures; $\overline{SA}$ is the mean structure obtained by averaging the coordinates of the individual SA structures best fitted to each other (excluding residues 1, 152, and 153); (SA)r is the restrained minimized mean structure obtained from $\overline{SA}$ (Nilges et al., 1988). The number of terms for the various restraints is given in parentheses. The target function that is minimized during the simulated annealing comprises quadratic harmonic potentials for covalent geometry (i.e., bonds, angles, planes, and chirality restraints), square-well quadratic potentials for the experimental distance and torsion angle restraints, and a quartic van der Waals repulsion term for the nonbonded contacts (Nilges et al., 1988). All peptide bonds were restrained to be trans with the exception of the Tyr-90–Pro-91 peptide bond, which was restrained to be cis on account of the observation of characteristic $C^{\alpha}H(i)$–$C^{\alpha}H(i+1)$ NOEs between these two residues (Clore et al., 1991). [b] None of the structures exhibited distance violations greater than 0.3 Å or dihedral angle violations greater than 2°. [c] For each backbone NH–CO hydrogen bond there are two restraints: $r_{NH-O} \leq 2.3$ Å and $r_{N-O} = 2.5$–3.3 Å. For each hydrogen bond between a backbone amide and a water molecule there are two restraints: $r_{NH-O} \leq 2.5$ Å and $r_{N-O} = 2.4$–3.5 Å, respectively; similarly, there are two restraints for each hydrogen bond between a backbone carbonyl and water: $r_{O-H} \leq 2.5$ Å and $r_{O-O} = 2.4$–3.5 Å. All hydrogen bonds involve slowly exchanging NH protons. [d] The values of the square-well NOE (F_{NOE}) and torsion angle (F_{tor}) potentials [cf. eqs 2 and 3 in Clore et al. (1986)] are calculated with force constants of 50 kcal·mol^{-1}·Å^{-2} and 200 kcal·mol^{-1}·rad^{-2}, respectively. The value of the quartic van der Waals repulsion term F_{rep} [cf. eq 5 in Nilges et al. (1988)] is calculated with a force cosntant of 4 kcal·mol^{-1}·Å^{-4} with the hard sphere van der Waals radius set to 0.8 times the standard values used in the CHARMM empirical energy function. [e] E_{L-J} is the Lennard-Jones van der Waals energy calculated with the CHARMM (Brooks et al., 1983) empirical energy function and is *not* included in the target function for simulated annealing or restrained minimization. [f] Internal residues are defined as those with ≤40% of the surface of the residue in a tripeptide Gly-X-Gly (Chothia, 1976) accessible in the calculated structures.

Table II: Summary of β-Strands

strand	residues	neighboring strands
I	5–12	XII–I–IV
II	17–22	II–III
III	25–30	II–III–XI
IV	40–52	I–IV–V
V	55–62	IV–V–VIII
VI	67–74	VI–VII
VII	77–85	VI–VII
VIII	99–106	V–VIII–IX
IX	109–114	VIII–IX–XII
X	120–125	XII–X–XI
XI	130–135	X–XI–III
XII	143–151	IX–XII–I

size can be found in a data bank of high-resolution protein X-ray structures (Jones & Thirup, 1986) that superimposes upon these irregular turns and short loops within a backbone atomic RMS difference of less than 0.5 Å. Strands III and IV are connected by an unusual 10-residue segment (residues 30–39) that comprises a type II turn (residues 32–35) followed by 2.3 turns of a 3_{10} helix (residues 33–39). The latter is characterized by four CO(i)–NH($i+3$) hydrogen bonds between residues 33 and 36, 34 and 37, 35 and 38, and 36 and 39. (Note that the NH protons of residues 36–39 are *not* slowly exchanging and that *no* hydrogen-bonding restraints for these hydrogen bonds were included in the calculations, so that their presence is solely a result of the interproton distance and torsion angle restraints.) Finally, strands VII and VIII are connected by a long 15-residue loop (residues 86–100) that contains two irregular type I turns (residues 86–89 and residues 97–100) and a type VIb turn (residues 89–92) with a *cis*-proline at position 90.

The stereoviews in Figure 3 correspond to the schematic representation of the topological units shown in Figure 3 of Clore et al. (1990b) and clearly illustrate their close structural similarity. Also shown in Figure 3 is the location of the seven bound water molecules associated (i.e., ≤3 Å) with the slowly exchanging backbone amide protons of Leu-10, Leu-18, Leu-26, Leu-60, Phe-112, Ser-125, Asn-129, and Met-130, all of which are not within hydrogen-bonding distance of any backbone or side-chain acceptor group. For slow amide proton exchange to occur, the water molecules must also exchange slowly with bulk solvent at the same rate as the NH exchange rate. This implies that each water molecule must be involved in at least two hydrogen bonds of the type NH···OH···O, where an NH group donates a hydrogen bond to the oxygen atom of the water and an acceptor group, usually a backbone carbonyl, accepts a hydrogen bond from one of the water protons. The identity of the acceptor group(s) can only be derived on the basis of the structure, and this is readily achieved by taking into account the known lengths of hydrogen bonds involving water molecules in proteins, the range of distances between an NH group and an acceptor group compatible with such hydrogen bonds (i.e., between 4 and 6 Å), and the known

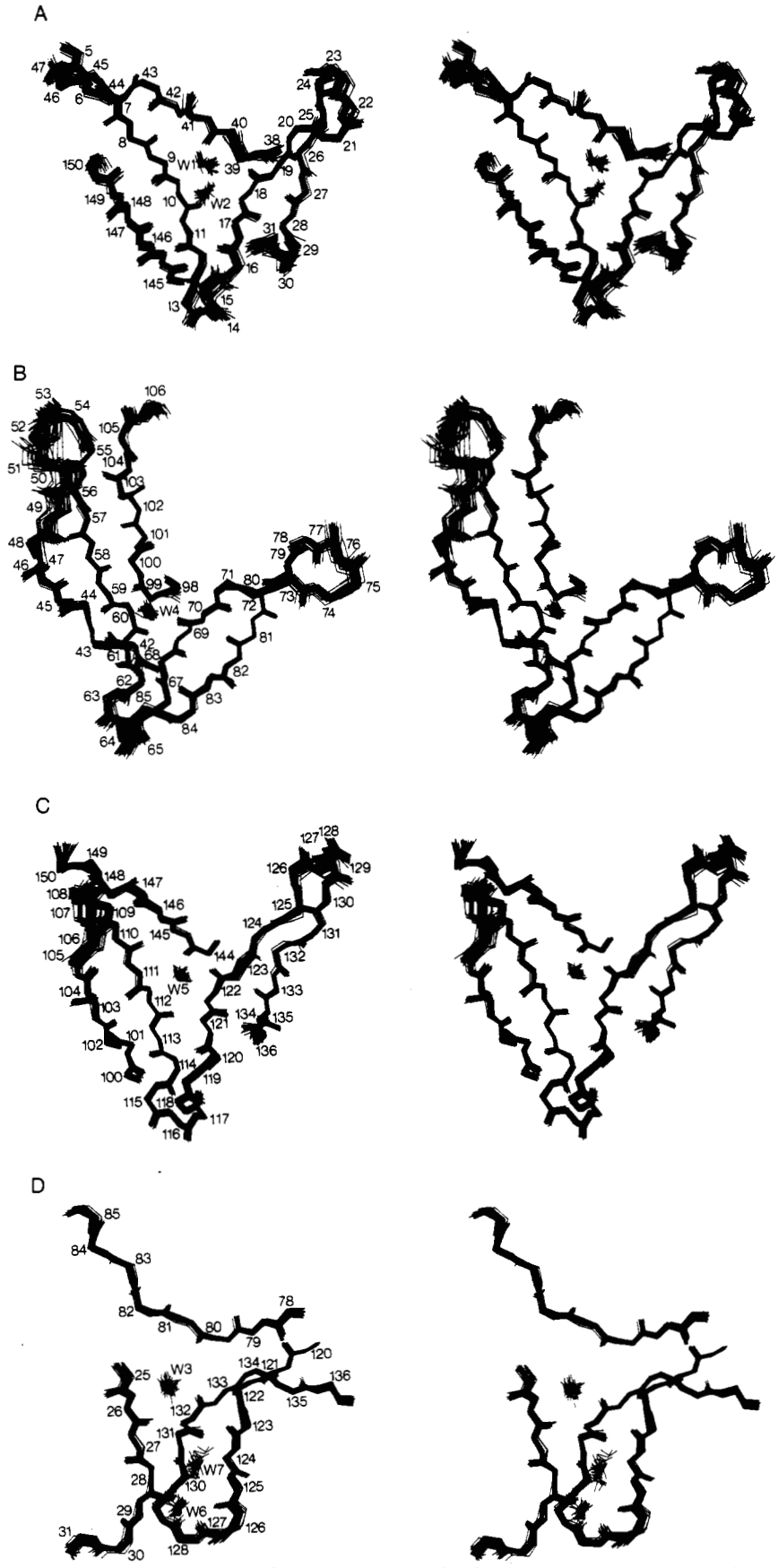

FIGURE 3: Stereoviews showing best fit superpositions of the backbone (N, C^{α}, C, O) atoms and water molecules of the 32 SA structures for the three repeating topological units of IL-1β (A–C) and the interface of the three units (D). Each topological unit is composed of five antiparallel β-strands.

directionality of hydrogen bonds (Baker & Hubbard, 1984). Consequently, these water molecules were only introduced in the *very last stage* of the refinement procedure. It must also be stressed that the introduction of the water molecules and the associated hydrogen-bonding restraints did *not* result in any increase in the precision of the structure determination, and the resulting atomic RMS shifts in the mean coordinate positions were very small (0.2 and 0.3 Å for the backbone and

all atoms of all residues, respectively, and 0.14 and 0.18 Å, respectively, when only internal residues with a surface accessibility of ≤40% are considered).

In topological unit A, Leu-10 NH in strand I and Leu-18 NH in strand II are close to bound water. After examination of the structure, it was clear that these two NH protons had to be associated with different water molecules. In particular, W1 is involved in bridging hydrogen bonds between Leu-10 NH and Val-40 CO (in strand IV), while W2 participates in bridging hydrogen bonds between Leu-18 NH and Leu-10 CO. In topological unit B, the water molecule (W4) hydrogen bonded to Leu-60 NH can clearly donate two hydrogen bonds, one to the backbone carbonyl of Leu-69 in strand VI and the other to the backbone carbonyl of Phe-99 in strand VIII. In topological unit C, the bound water molecule (W5) displays exactly the same sort of hydrogen-bonding interactions as in topological unit B. In particular, W5 accepts a hydrogen bond from the NH of Phe-112 in strand IX and donates two hydrogen bonds to the backbone carbonyls of Ile-122 in strand X and Thr-144 in strand XII. At the interface of the three units, which is formed by strands III, VII, and IX, the water molecule W3 bridges the NH of Leu-26 in strand III and the backbone carbonyl of Val-132 in strand IX. Examination of Figure 3 clearly shows that these five bound water molecules occupy very similar spatial positions in the three topological units and at the interface of the three units, thereby playing an important role in stabilizing the structure. In this regard, it is noteworthy that three of the associated NH protons, namely, those of Leu-10, Leu-60, and Phe-112, are among the most slowly exchanging NHs in the whole protein with half-lives of more than 3 days (Driscoll et al., 1990b). In addition to these five water molecules, there are two other bound waters involved in stabilizing the loop between strands X and XI. In particular, W7 bridges a hydrogen bond between the NH of Ser-125 and the CO of Met-130 at the base of the loop, while W6 accepts hydrogen bonds from the NHs of Asn-129 and Met-130 and donates hydrogen bonds to the backbone carbonyls of Ala-127 and Ala-28. The latter interaction serves to stabilize the orientation of this loop with regard to strand III.

The exterior of the protein is charged and hydrophilic, while the interior is highly hydrophobic. Nevertheless, of the 14 most buried residues (surface accessibility ≤3%, ≤5 Å^2), seven are hydrophilic in nature, comprising two Cys (Cys-8 and -71), three Ser (Ser-70, -114, and -123), one Thr (Thr-124), and one Asp (Asp-12). The inaccessibility of the two Cys residues (which are not disulfide bridged and are separated by ~16 Å) accounts for their complete lack of reactivity toward sulfhydryl reagents in the native protein (Wingfield et al., 1986). In the main, the buried hydrophilic residues are involved in hydrogen-bonding or electrostatic interactions. The carboxylate of Asp-12 (strand I) participates in three hydrogen-bonding interactions with the backbone amides of Gln-14 and Lys-16 and the hydroxyl group of Thr-124. The first two hydrogen bonds serve to stabilize the turn between strands I and II, while the third is important in positioning strands I and II relative to strands X and XI (Figure 1A). The SH group of Cys-71 (in strand VI) is hydrogen bonded to the hydroxyl group of Ser-114 (in strand IX), the hydroxyl group of Ser-70 (strand VI) is hydrogen bonded to the carboxylate side chain of Glu-83 in the adjacent strand (strand VII), and in strand X the hydroxyl group of Ser-123 is hydrogen bonded to the backbone carbonyl of Tyr-121.

The packing of some of the internal residues with respect to one another, as well as the excellent definition of internal side chains, is illustrated in Figure 4. Hydrophobic interactions are crucial in tethering the external strands, turns, and loops to the barrel. For example, residues 71–80, which comprise the end of strand VI and the beginning of strand VII, together with the type I′ turn between them, appear to be highly exposed to solvent (Figure 1B), yet their orientation with respect to the core of the protein is stabilized by numerous interactions involving strands VII, IX, X, and XI, as well as the loop connecting strands IX and X (Figure 4A). Thus, the buried Cys-71 is in close proximity to Leu-134 in strand XI, Leu-73 and Pro-78 interact with Phe-117, which is located in the loop between strands IX and X, and Leu-80 is close to Ile-122 in strand X. Further, Pro-78 is sandwiched between Phe-117 and Trp-120 (Figure 4A), which not only accounts for the extreme upfield shift of the ^{1}H resonances of Pro-78 (Clore et al., 1990a) but is also important in fixing the position of the connecting loop between strands X and XI (residues 115–120). In addition, the position of the exposed turn comprising residues 74–77 is stabilized by an electrostatic interaction between the $N^{\zeta}H_3^+$ of Lys-74 and the amino group of Gln-81 in strand VII. Another highly exposed loop is that between strands XI and XII (residues 136–141; Figure 1A). In this case Trp-120 in strand X is closely packed against Gly-135 and -136, and there is a salt bridge between Lys-138 and Glu-111 (strand IX). In addition, the beginning of strand XII is tethered by hydrophobic interactions between Ile-143, Ser-13 (strand I), and Thr-124 (strand X), and between Thr-144 and Tyr-121 (strand X), and by an electrostatic interaction between the side chains of Asp-145 and Ser-13.

A similar dense network of interactions is found for the other loops. For example, the connecting segment between strands III and IV (residues 30–39) is stabilized by hydrophobic interactions between Leu-31 and residues in strands II (Val-19) and III (Leu-29), and the 3_{10} helix (residues 33–39) is further stabilized by an electrostatic interaction between the side-chain carboxylate of Asp-35 and the amino group of Gln-38. The short loop (residues 51–56) between strands IV and V is stabilized by hydrophobic interactions with residues on strand VIII: namely, between the aliphatic portion of the side chain of Lys-53 and Ile-104 and between Ile-56 and the aliphatic portion of the side chain of Lys-103. The short loop between strands V and VI (residues 62–67) is stabilized by hydrophobic interactions between Leu-62, Leu-67, and residues in strands III (Tyr-24, Leu-26), IV (Val-40, Phe-42), and VII (Leu-80) (Figure 4A,C).

In the case of the long loop between strands VII and VIII (residues 86–100), Val-85, Tyr-90, and Phe-99 are close to Tyr-68 in strand VI (Figure 4A,C), Met-95 is close to hydrophobic residues in strands IV (Val-47) and V (Ala-59), there is a potential electrostatic interaction between the side chain of Asn-66 (strand VI) and the backbone nitrogen atom of Pro-87, and finally there is a backbone hydrogen bond between the NH of Gln-48 (strand IV) and the carbonyl oxygen of Lys-93. In addition, some of the local features such as the two type I turns are stabilized by short-range electrostatic interactions, in particular between the side chains of Asp-86 and Asn-89 and between Glu-96 and Arg-98.

The short loop between strands X and XI (residues 125–130) displays two side-chain–side-chain electrostatic interactions with residues on strand III, namely, between Glu-128 and His-30 and between Asn-129 and Lys-27. In this regard it is interesting to note that although His-30 is exposed to solvent (cf. Figure 2A), it displays a high pK of 7.5 (Gronenborn et al., 1986), which can be attributed to its interaction with the negatively charged carboxylate of Glu-128.

Comparison with the X-ray Structure. At approximately the same time as the sequential assignments and secondary

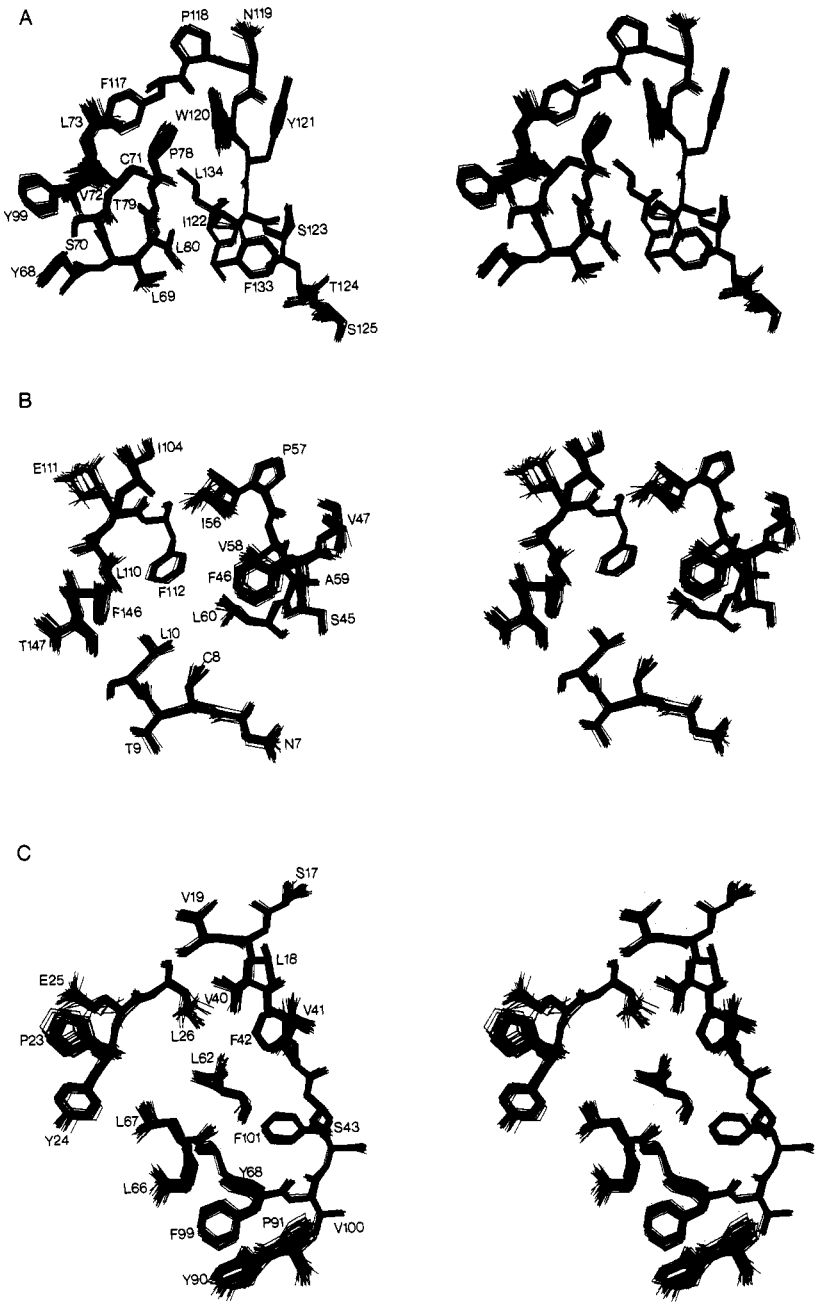

FIGURE 4: Stereoviews showing best fit superpositions of all atoms (excluding protons) of the 32 SA structures for three selected segments of IL-1β.

structure determination of IL-1β were published (Driscoll et al., 1990a,b), two refined X-ray structures of IL-1β at 2-Å resolution were determined by two groups independently (Finzel et al., 1989; Priestle et al., 1989). A detailed comparison with the X-ray structures will be published elsewhere, so that only a brief overview is presented here. The atomic RMS difference between the restrained minimized average NMR structure ($\overline{SA}$)r and the X-ray structure of Finzel et al. (1989) is 0.85 Å for the backbone atoms and 1.3 Å for all atoms. When only internal residues (≤40% surface accessibility) are considered, these values drop to 0.68 and 1.0 Å, respectively. The most significant structural difference lies in the distance from the tip of the loop (residues 32–36) connecting strands III and IV to strands I and XII, which is about 1 Å less in the case of the X-ray structure than of the NMR one. This difference can be attributed to a hinge motion about residues 31 and 36 and is in all likelihood due to intermolecular crystal packing contacts in this region (Finzel et al., 1989).

Relationship of Structure to Function. At the present time a number of mutational and chemical modification studies on IL-1β have been published and the receptor binding and/or biological activity characterized. With the solution NMR structure in hand, some of these results can be interpreted in structural terms.

Several lines of evidence indicate that the large concave face of the molecule formed by residues 19–27 (strands II to III), 70–84 (strands VI and VII), and 121–142 (strand X to the beginning of strand XII) is not involved in receptor binding. This face is located at the "back" of the molecule on the opposite side to the front end of the β-barrel (i.e., at the back of Figure 1A). First, mutations of Tyr-24 → Phe, Lys-27 → Cys, Trp-120/Tyr-121 → Phe/Phe, and Lys-138 → Cys have no effect on receptor binding (MacDonald et al., 1986; Wingfield et al., 1989). Second, derivatization of the Lys-77 → Cys mutant with an ~60-kDa biotin–streptavidin complex through the surface-accessible SH group has no effect on receptor binding (A. Chollet and P. T. Wingfield, unpublished

data). Similarly, derivatization of the Lys-138 → Cys mutant with phycobiliprotein, a protein of 240-kDa, does not affect receptor binding (Wingfield et al., 1989).

Mutants that influence either receptor binding and/or activity are located in three distinct regions of the molecule. The first region comprises the N- and C-termini, which are located close together in space (Figure 1A). While removal of the N-terminal residues up to but excluding Arg-4 has little effect on receptor binding (Kamogashira et al., 1988; P. T. Wingfield, unpublished data), mutation of Arg-4 to either Glu (Huang et al., 1987) or Asp (Kamogashira et al., 1988) reduces both receptor binding and activity almost 1000-fold. The importance of the N-terminus is further highlighted by two additional pieces of evidence. First, receptor binding of the unprocessed N-terminal methionylated IL-1β is 10-fold lower than that of the mature protein (Wingfield et al., 1987), and second, derivatization of a mutant in which a cysteine was inserted between Ala-1 and Pro-2 with streptavidin leads to the complete abolition of receptor binding (A. Chollet and P. T. Wingfield, unpublished data). Similarly, deletion of more than the last three residues at the C-terminus severely reduces receptor binding (Mosley et al., 1987; Kamogashira et al., 1988). Examination of the surface of the protein reveals a potential binding cleft (located on the right-hand side of Figure 1A) with a radius of ~8 Å comprising the following surface-accessible residues: Arg-4 and Leu-6 from strand I, Phe-46 from strand IV, Ile-56 from strand V, Lys-103 and Glu-105 from strand VIII, Asn-108 and Leu-110 from strand IX, and Met-148 and Phe-150 from strand XII.

The second region is characterized by mutations of Arg-11 and His-30. The Arg-11 → Gly mutant displays a very small (~25%) reduction in receptor binding but a 100-fold reduction in biological activity (Gehrke et al., 1990). The His-30 → Asn and His-30 → Arg mutants exhibit 30- and 100-fold reductions, respectively, in receptor binding (MacDonald et al., 1986). Both the residues are located in a possible second binding cleft on the molecule located at the bottom left-hand side of Figure 1A. This site has a radius of ~7 Å and comprises Arg-11 and Gln-15 from strand I, His-30, Gln-32, Met-36, and Gln-39 from the segment connecting strands III and IV (which comprises the 3_{10} helix from residues 33–39), and Gln-149 from strand XII at the C-terminus. A ridge-like border between this site and the first one is formed by strand XII. It is also interesting to note that the decrease in receptor binding affinity produced by the presence of both the N-terminal Met and the His-30 → Arg mutation is additive rather than synergistic (Wingfield et al., 1987), providing further evidence that sites 1 and 2 constitute two distinct receptor-binding sites.

The third site is defined by the mutation of Asp-145 → Lys, which has minimal effects on receptor binding but reduces biological activity significantly (Ju et al., 1991). This cleft has a radius of 5–6 Å and is located at the top left of Figure 2A and at the top middle of Figure 2B. It is formed by Ser-13 and Gln-14 of strand I, Lys-109 of strand IX, Gln-126 of strand X, and Asp-145 of strand XII. The border between the third and first binding sites is formed by the turn (residues 105–108) between strands VIII and IX, while the border with the second site is formed by the turn (residues 12–15) between strands I and II.

These three regions occupy a large surface area of the protein. For example, the distances between His-30 and Arg-4, Asp-145 and Arg-4, and His-30 and Asp-145 are ~33, ~26, and ~14 Å, respectively. Interestingly, the amino acid sequence of the extracellular ligand-binding portion of the IL-1β receptor reveals three immunoglobulin-like domains, all of which may be required for receptor binding and/or biological activity (Sims & Dower, 1990). This suggests that each domain of the receptor may bind to one of the three postulated receptor-binding sites on IL-1β and, in the light of the mutational data, leads one to speculate that the first site contributes most of the binding energy, while the second and third sites may play a role in signal transduction, internalization of the IL-1β–IL-1 receptor complex, and cellular and nuclear targeting.

ACKNOWLEDGMENTS

We thank Dr. Ad Bax for many useful and enlightening discussions and Dr. B. C. Finzel for providing us with the coordinates of the crystal structure of IL-1β.

REFERENCES

Brooks, B. R., Bruccoleri, R. E., Olafson, B. D., States, D. J., Swaminathan, S., & Karplus, M. (1983) *J. Comput. Chem. 4*, 187–217.

Brünger, A. T. (1988) *XPLOR Manual*, Yale University, New Haven, CT.

Chothia, C. (1976) *J. Mol. Biol. 105*, 1–14.

Clore, G. M., Nilges, M., Sukumaran, D. K., Brünger, A. T., Karplus, M., & Gronenborn, A. M. (1986) *EMBO J. 5*, 2729–2735.

Clore, G. M., Gronenborn, A. M., Nilges, M., & Ryan, C. A. (1987) *Biochemistry 26*, 8012–8013.

Clore, G. M., Bax, A., Driscoll, P. C., Wingfield, P. T., & Gronenborn, A. M. (1990a) *Biochemistry 29*, 8172–8184.

Clore, G. M., Bax, A., Wingfield, P. T., & Gronenborn, A. M. (1990b) *Biochemistry 29*, 5671–5676.

Clore, G. M., Driscoll, P. C., Wingfield, P. T., & Gronenborn, A. M. (1990c) *Biochemistry 29*, 7387–7401.

Clore, G. M., Driscoll, P. C., Wingfield, P. T., & Gronenborn, A. M. (1990d) *J. Mol. Biol. 214*, 811–817.

Clore, G. M., Appella, E., Yamada, M., Matsushima, K., & Gronenborn, A. M. (1990e) *Biochemistry 29*, 1689–1696.

Clore, G. M., Kay, L. E., Bax, A., & Gronenborn, A. M. (1991a) *Biochemistry 30*, 12–18.

Clore, G. M., Bax, A., & Gronenborn, A. M. (1991b) *J. Biomol. NMR* (in press).

Dinarello, C. A. (1989) *Adv. Immunol. 44*, 153–205.

Driscoll, P. C., Clore, G. M., Marion, D., Wingfield, P. T., & Gronenborn, A. M. (1990a) *Biochemistry 29*, 3542–3556.

Driscoll, P. C., Gronenborn, A. M., Wingfield, P. T., & Clore, G. M. (1990b) *Biochemistry 29*, 4468–4682.

Dyson, H. J., Gippert, G. P., Case, D. A., Holmgren, A., & Wright, P. E. (1990) *Biochemistry 29*, 4129–4136.

Finzel, B. C., Clancy, L. L., Holland, D. R., Muchmore, S. W., Watenpaugh, K. D., & Einspahr, H. M. (1989) *J. Mol. Biol. 209*, 779–791.

Forman-Kay, J. D., Clore, G. M., Wingfield, P. T., & Gronenborn, A. M. (1991) *Biochemistry* (in press).

Gehrke, L., Jobling, S. A., Paik, L. S. K., McDonald, B., Rosenwasser, L. J., & Auron, P. E. (1990) *J. Biol. Chem. 265*, 5922–5925.

Gronenborn, A. M., Clore, G. M., Schmeissner, U., & Wingfield, P. T. (1986) *Eur. J. Biochem. 161*, 37–43.

Havel, T. F. (1986) *DISGEO, Quantum Chemistry Program Exchange No. 507*, Indiana University, Bloomington, IN.

Huang, J. J., Newton, R. C., Horuk, R., Matthew, J. B., Covington, M., Pezzella, K., & Lin, Y. (1987) *FEBS Lett. 223*, 294–298.

Ikura, M., Kay, L. E., Tschudin, R., & Bax, A. (1990) *J. Magn. Reson. 86*, 204–209.

Jones, T. A., & Thirup, S. (1986) *EMBO J. 5*, 819–822.
Ju, G., Campen, C. A., Benjamin, W. R., Labriola-Tompkins, E., Karas, E., Plocinski, J., Biondi, D., Kaffka, K., Kilian, P. L., Eisenberg, S. P., & Evans, R. J. (1991) *Proc. Natl. Acad. Sci. U.S.A.* (in press).
Kamogashira, T., Sakaguchi, M., Ohmoto, Y., Mizuno, K., Shimizu, R., Nagamura, K., Nakai, S., Masui, Y., & Hirai, Y. (1988) *J. Biochem. (Tokyo) 104*, 837–840.
Kay, L. E., & Bax, A. (1989) *J. Magn. Reson. 86*, 110–126.
Kay, L. E., Clore, G. M., Bax, A., & Gronenborn, A. M. (1990) *Science 249*, 411–414.
Kraulis, P. J., Clore, G. M., Nilges, M., Jones, T. A., Petterson, G., Knowles, J., & Gronenborn, A. M. (1989) *Biochemistry 28*, 7241–7257.
MacDonald, H. R., Wingfield, P. T., Schmeissner, U., Shaw, A., Clore, G. M., & Gronenborn, A. M. (1986) *FEBS Lett. 209*, 295–298.
Marion, D., Kay, L. E., Sparks, S. W., Torchia, D. A., & Bax, A. (1989a) *J. Am. Chem. Soc. 111*, 1515–1517.
Marion, D., Driscoll, P. C., Kay, L. E., Wingfield, P. T., Bax, A., Gronenborn, A. M., & Clore, G. M. (1989b) *Biochemistry 28*, 6150–6156.
Mosley, B., Dower, S. K., Gillis, S., & Cosman, D. (1987) *Proc. Natl. Acad. Sci. U.S.A. 84*, 4572–4576.
Mueller, L. (1987) *J. Magn. Reson. 72*, 191–196.
Nilges, M., Clore, G. M., & Gronenborn, A. M. (1988) *FEBS Lett. 229*, 317–324.
Nilges, M., Clore, G. M., & Gronenborn, A. M. (1990) *Biopolymers 29*, 813–822.
Priestle, J. P., Schär, H.-P., & Grütter, M. (1989) *Proc. Natl. Acad. Sci. U.S.A. 86*, 9667–9671.
Qian, Y. Q., Billetter, M., Otting, G., Müller, M., Gehring, W. J., & Wüthrich, K. (1989) *Cell 59*, 573–580.
Shaka, A. J., Lee, C. J., & Pines, A. (1988) *J. Magn. Reson. 77*, 274–293.
Sims, J. E., & Dover, S. K. (1990) in *The Year of Immunology 1989–1990* (Cruse, J. M., & Lewis, R. E., Eds.) Vol. 6, pp 112–126, Karger, Basel.
Wingfield, P. T., Payton, M., Tavernier, J., Barnes, M., Shaw, A., Rose, K., Simona, M. G., Demaczuk, S., Williamson, K., & Dayer, J.-M. (1986) *Eur. J. Biochem. 160*, 491–497.
Wingfield, P. T., Graber, P., Movva, N. R., Clore, G. M., Gronenborn, A. M., & MacDonald, H. R. (1987) *FEBS Lett. 215*, 160–164.
Wingfield, P. T., Graber, P., Shaw, A. R., Gronenborn, A. M., Clore, G. M., & MacDonald, H. R. (1989) *Eur. J. Biochem. 179*, 565–571.
Wüthrich, K., Billetter, M., & Braun, W. (1983) *J. Mol. Biol. 169*, 949–961.
Zuiderweg, E. R. P., & Fesik, S. W. (1989) *Biochemistry 28*, 2387–2391.
Zuiderweg, E. R. P., McIntosh, L. P., Dahlquist, F. W., & Fesik, S. W. (1990) *J. Magn. Reson. 86*, 210–216.

Articles

X-ray Absorption Fine Structure Investigation of the Zinc Transition Metal Binding Site of Zn Concanavalin A in Solution and in the Crystal†

S.-L. Lin,‡ E. A. Stern,*,‡ A. J. Kalb (Gilboa),§ and Y. Zhang‡

Department of Physics FM-15, University of Washington, Seattle, Washington 98195, and Department of Biophysics, Weizmann Institute of Science, Rehovoth, Israel

Received September 6, 1990; Revised Manuscript Received December 4, 1990

ABSTRACT: We report details on measurements by the X-ray absorption fine structure (XAFS) technique of the conformational changes around the transition metal binding site (S1) of the protein concanavalin A induced by crystallization when that site is occupied by Zn. A change from hexa- to tetracoordination occurs at the S1 site on crystallization when the calcium-binding site (S2) is occupied by a calcium atom. When the S2 site is unoccupied, the Zn is pentacoordinated both in solution and in the crystal. The average distance to the coordination shell increases with coordination number as expected. Conformational changes are detected up to 4.5 Å from the Zn, the limit of sensitivity of the XAFS technique. When the Zn is hexacoordinated, the ligands around the Zn, as determined by XAFS, are consistent with the crystal structure determination results of five oxygens and one nitrogen. The atom that is released when the coordination decreases to five is an oxygen atom, and, in addition, the nitrogen is released in the tetracoordinated Zn. Thus, when S2 is emptied, the protein gains a ligand about the Zn site in the crystal and loses one in solution. These results provide direct evidence that the protein conformation can be altered by the intermolecular forces of crystallization.

The foundation of our understanding of the mechanism of the functioning of proteins is knowledge of their structure, and almost all of the information on protein structure has come from X-ray diffraction studies on the crystalline state. Recently we reported structural differences in the protein concanavalin A between its solution and crystal forms (Lin et al., 1990). This finding raises once more the question of how generally one can relate the crystalline structure of proteins to their behavior in solution. Although our recent XAFS work is the first that *directly* compared the structure of a protein in a crystal and in solution by the same technique, there have been other indications of structural differences in proteins

† This work was funded by NSF under Grant DMB-8613948.
‡ University of Washington.
§ Weizmann Institute of Science.

0006-2960/91/0430-2323$02.50/0